Near-Infrared Surface Photometry of Bulges and Disks of Spiral Galaxies. The Data

R. F. Peletier[1,2]

M. Balcells[2,1]
[1]Kapteyn Astronomical Institute, Postbus 800, 9700 AV Groningen, Netherlands
[2]Instituto de Astrofísica de Canarias,E-38200 La Laguna, Tenerife, Spain

ABSTRACT

We present optical and near-infrared (NIR) surface brightness and colour profiles, in bands ranging from U to K, for the disk and bulge components of a complete sample of 30 nearby S0 to Sbc galaxies with inclinations larger than 50°. We describe in detail the observations and the determination of colour parameters. Calibrated monochromatic and real-colour images are presented, as well as colour index maps. This data set, tailored for the study of the population characteristics of galaxy bulges, provides useful information on the colours of inner disks as well. In related papers, we have used them to quantify colour gradients in bulges, and age differentials between bulge and inner disk.

Subject headings: Galaxies:Bulges; Galaxies:Disks; Galaxies:Ages; Galaxies:Populations

1. Introduction

In a recent series of papers we analyze various structural and population parameters of the bulge component of early-to-intermediate type disk galaxies. We did this by obtaining and analyzing accurate surface photometry of a complete sample of inclined spiral galaxies. In Balcells & Peletier (1994, hereafter BP94) we derive optical colour profiles and compare mean colours and colour gradients of bulges to those of ellipticals. We find that bulges have similar or bluer colours than ellipticals of the same luminosity, implying that many bulges contain younger populations, or have lower metallicity, than corresponding ellipticals. In Peletier & Balcells (1996a, hereafter PB96a) we compare the colours of bulges to those of inner disks. These two colours not only scale with each other, a result already shown in BP94; colours of bulges and inner disks are almost identical; the bulge does not appear as a morphological component in colour index maps. Implied age differences are very small, with dlog(age) ranging from 0 to 0.15. This result, derived from NIR as well as optical data, is not affected by uncertainties due to dust extinction in the disk. Finally, in Andredakis, Peletier & Balcells (1995, hereafter APB95) we develop a 2D bulge-disk decomposition, an extension of Kent's (1984) method, and show that surface brightness profiles of bulges follows an $r^{1/n}$ law, with n ranging from 4-6 for S0's to 1 for Sc's. In a future paper (Peletier & Balcells, in preparation) we will discuss optical-infrared colour gradients in bulges and disks; some of these results have already been presented in Peletier & Balcells (1996b, hereafter PB96b).

The validity of these results rests first on the quality of the raw data, and second on the attention given to the problem of dust extinction. The latter is described in detail in the previous papers in this series. As for the data, we were fortunate that photometric conditions pervailed during both the optical and NIR observations; flat-fielding, critical for sky subtraction, was accurate to about 0.2% of the sky, and

a factor 10 better in the near-infrared. The sample is complete for the specified galaxy types and diameter and magnitude ranges.

Optical and NIR colours of nearby galaxies contain important clues on the star formation history of spiral galaxies. Not only can one learn about the stellar contents of these objects, but also, by comparing the properties with galaxies at large redshift one can study the evolution of stellar populations. In the last few years several studies of the colours of spiral galaxies have appeared. Terndrup *et al.* (1994) observed 43 galaxies in J and K, which was complemented with r-band photometry of Kent (1984, 1986, 1987). De Jong & van der Kruit (1994) and de Jong (1996) published B, V, R, I and K-band photometry of 86 spiral galaxies. Both samples contain nearby spirals of types S0 - Sc, while de Jong's sample only contains face-on or nearly face-on galaxies. Peletier *et al.* (1994) imaged 37 galaxies in the K-band, and combined this with B and R-band images of the ESO-LV catalog (Lauberts & Valentijn 1989). Their sample only contains galaxies of types Sb-Scd, at somewhat larger distances and smaller, and which are likely to be severely affected by extinction by dust. The current sample is complementary in type to it, and is complementary to de Jong's sample in inclination.

The fact that our sample is biased towards early-type spiral galaxies, with large bulges, the high inclination on the sky, the good sampling, the relative novelty of the near-infrared data, and especially the fact that we have good-quality surface photometry in 6 bands, makes this data set ideal to study the colour properties of bulges and inner disks of early-type spiral galaxies. Using the opportunities of a new electronic medium we present here all of the available data in graphical and tabular form. In § 2. we describe the sample and the optical and NIR observations. In § 3. we describe the complete process of obtaining optical and NIR colour profiles. In § 3.6. we compare our results to NIR aperture photometry and to published NIR colour profiles. A discussion of the data quality is given in § 4..

2. Observations

2.1. The Sample

Our initial goal, that of obtaining colour information on bulges, made us select galaxies at high inclinations ($i > 50^o$), in order to minimize the the amount of disk light which projects onto the bulge, and to ensure that extinction from dust in the disk does not dominate the colours measured on the bulge. We chose early-to-intermediate type spiral galaxies. Dust extinction is important at high inclinations, but it is confined to the side of the galaxy were the disk is seen in front of the bulge, leaving the other side largely unobscured. We started with a sample of 45 galaxies, comprising all galaxies with right ascension between 13^h and 24^h, declination above –2°, galaxy type earlier than Sc, excluding barred galaxies, apparent blue magnitude brighter than 14.0, major axis diameter larger than 2 arcmin, absolute galactic latitude larger than 20° and axis ratio in B larger than 1.56. Subsequent examination of the individual images during the run led to the exclusion of 12 objects: NGC 5935, 5930, 6207, 6585, 6796, 7177, 7286, 7428, 7463, 7753, and UGC 9483, 10713, due to being barred, very patchy all the way to the center, irregular, or belonging to interacting systems (see BP94). NGC 7331 was not considered due to its large size. Finally, two of the remaining 32 galaxies were too far North to be observed from UKIRT: NGC 5308 and NGC 6361. All galaxies except NGC 5675 were observed in U, B, R, I and K; 20 out of 30 were observed in J. The sample is given in Table 1.

Table 1: THE SAMPLE

UGC	NGC	Type	ϵ	M_R^{tot}	M_R^{bul}	B/D	J	PA
(1)	(2)	(3)	(4)	(5)	(6)	(7)	(8)	(9)
8764	5326	1	0.50	–22.16	–21.22	0.73	Y	-138
8835	5362	3	0.62	–20.92	–	0.00	Y	2
8866	5389	0	0.80	–21.32	–20.70	1.30	Y	93
8935	5422	–2	0.80	–21.96	–21.33	1.28	Y	64
8958	5443	3	0.68	–21.53	–19.09	0.12	Y	-52
9016	5475	0	0.68	–20.98	–18.72	0.14	Y	-101
9187	5577	4	0.72	–20.51	–17.34	0.06	Y	-38
9202	5587	0	0.70	–21.07	–19.43	0.29	N	73
9357	5675	0	0.68	–22.17	–	0.00	N	47
9361	IC1029	3	0.76	–21.92	–20.66	0.46	N	-119
9399	5689	0	0.75	–22.29	–21.47	0.89	Y	-5
9428	5707	2	0.75	–21.43	–20.11	0.42	N	-59
9462	5719	2	0.64	–21.60	–20.00	0.30	N	5
9499	5746	3	0.84	–22.68	–21.70	0.68	Y	-99
9692	5838	–3	0.65	–21.89	–20.93	0.71	Y	134
9723	5866	–1	0.60	–21.71	–19.80	0.21	Y	-144
9726	5854	–1	0.70	–21.43	–20.18	0.46	Y	-33
9753	5879	4	0.62	–20.30	–19.08	0.48	Y	89
9805	5908	3	0.78	–22.88	–22.04	0.85	N	61
9914	5965	3	0.84	–22.92	–21.76	0.53	Y	-38
9971	5987	3	0.60	–22.96	–21.54	0.37	Y	-29
10081	6010	0	0.75	–21.57	–19.88	0.27	Y	12
10856	6368	3	0.80	–22.43	–21.16	0.45	Y	-179
11053	6504	2	0.83	–24.57	–23.30	0.45	N	135
11401	6757	0	0.60	–24.60	–22.64	0.20	N	177
12080	7311	2	0.50	–23.43	–22.30	0.55	N	-75
12115	7332	–2	0.74	–21.86	–20.52	0.41	Y	-114
12306	7457	–3	0.48	–20.91	–20.91	10.00	Y	35
12442	7537	4	0.66	–21.37	–19.53	0.23	Y	170
12691	7711	–2	0.56	–22.63	–22.63	10.00	Y	-178

Notes to table 1: Description of the columns:
(1) and (2): the UGC and NGC numbers of the galaxies.
(3): Type index T from the *Third Reference Catalogue of Bright Galaxies* (de Vaucouleurs et al. 1991, hereafter RC3).
(4): disk ellipticity derived from elliptical fits to our R-band images.
(5) and (6): absolute magnitudes derived from our R-band photometry and the velocities listed in the RC3 (uniform Hubble flow with $H_0 = 50$ km s^{-1} Mpc^{-1}).
(7): bulge-to-disk ratio derived from an R-band bulge-disk decomposition following Kent's (1984) method.
(8): observed in J (Y) or not.
(9): the position angle (N – E) of the dust-free minor axis.

2.2. Optical Observations

Broad band CCD U, B, R and I images were obtained with the PF camera of the Isaac Newton telescope in June 1990. The optical observations are described in detail in BP94. We used a coated 400×590 GEC chip with pixel size of 0.549 arcsec. Typical exposure times ranged from 1200 sec in U to 200 sec in R and I. Flat-fielding was better than 0.2%. Linearity of the chip response was better than 1% over the entire intensity range. Sky transparency was good and stable during the whole run. Absolute photometric errors were around 0.05 mag in R and I, and 0.10 mag in B and U. The effective seeing as measured on stellar images ranges between 1.0 and 1.5″ .

2.3. Near-Infrared Observations

The NIR observations were taken on June 2-5, 1994 at UKIRT at Mauna Kea, Hawaii, using IRCAM3, a camera equipped with a 256 × 256 InSb detector. A brief description of the observations is given in PB96a. The pixelsize, as measured on the frames, was 0.291″ . The detector was cosmetically very clean, with less than 1% bad pixels. Details can be found in Puxley & Aspin (1994). Although relatively large for an infrared camera, the field of IRCAM3 is still small to cover these large galaxies. For each galaxy we observed a sequence of 10 frames: 6 frames of the galaxy, with the center each time at a different place, and 4 of the neighbouring background sky. For reduction, we first applied a linearity correction to all the data. This correction was determined from a sequence of frames of the inside of the dome with a range of exposure times. At the high intensity levels this correction reached 6%. Following this a median filtered sky frame was made of the 4 sky-images. This frame was scaled and subtracted from each of the object frames. Following this the object frames were flatfielded using a flatfield obtained from all dark sky frames of that night. Our experience is that for this kind of InSb array these flatfields are of the same quality as dome flatfields. Finally, a mosaic was made by combining the 6 frames, using the galaxy center as the reference point, and adjusting the sky background of each frame individually. Details about how the mosaics were made can be found e.g. in Peletier (1994). The final mosaics have a size of aproximately 120 × 100″. Since the galaxies are inclined to the line-of-sight, the mosaics are large enough to determine and subtract the residual sky background for most of the galaxies. The seeing FWHM, as measured on bright stars in the images, ranges from 0.8 to 1.2″. Our typical integration times per readout were 6 or 10s in K and 10 or 20s in J. After typically 90s the coadded frame was written to disk and the telescope moved to a slightly different position.

The conditions were photometric during the 2nd and 3rd night. During these two nights we reobserved briefly all galaxies of the first night, to obtain photometric zero points. During each of the last two nights, we observed 8-10 UKIRT faint standard stars of the list of Casali (unpublished), with at least 4 observations per standard star in different positions on the chip. The RMS accuracy of the standard star observations was 0.03 mag in K and 0.035 mag in J. The $J-K$ colour term was negligible. In the infrared no corrections were made for galactic extinction and no K-correction because of redshift of the spectrum was applied. These corrections however were made in the optical (see BP94).

3. Data reduction

3.1. Near-infrared data reduction

Essential in the derivation of NIR mosaics is to derive good estimates for the sky background. Terndrup *et al.* (1994) discuss this point extensively. The variability in the sky, on levels of 10 - 100% in the near-infrared in the course of one night and on levels of percents during the taking of the mosaic, is so large that a residual sky background had to be determined on the final mosaic. Fortunately, IRCAM3 is very stable, as compared to for example 256 × 256 HgCdTe detectors, making flatfielding to better than 0.1% easily possible. As a test, we divided 2 sky-frames, taken 10 minutes apart, by each other, after having subtracted the dark current. The non-random non-uniformities on scales of $\sim 10 - 20$" are about 0.05%. In our case, where we take first three galaxy-frames, then four sky-frames, and then three galaxy-frames, and where we first subtract the median of the sky's before flatfielding, we were in general able to achieve an accuracy of 0.02% of sky. When the conditions were not photometric, i.e. during parts of the first night, the flatfielding accuracy is somewhat worse.

Even though we use a larger format array than has been done in the past, and even after mosaicing, some galaxies are larger than the entire frame. In these cases, the sky determination is most probably an overestimate. We estimate by how much by taking a much larger I-band frame, assuming that the colour gradients are small in the outer parts, and measuring the contribution in I at about 50" from the center on the galaxy's minor axis. This contribution in J and K generally corresponds to a surface brightness level between 23 and 25 mag/sq. arcsec in J and between 22 and 24 mag/sq. arcsec in K. Although different from galaxy to galaxy, a 1σ error in the sky corresponds in U, B, R, I, J and K appr. to resp 28.0, 29.0, 27.0, 26.0, 23.0 and 21.7 mag/sq. arcsec (for details about the numbers in the optical see BP94).

3.2. Optical and NIR colour profiles

After reduction we rotated and rebinned the J and K mosaics to align them with the optical images. The scaling and rotation was determined on some frames with many stars, then applied to all the NIR frames. The frames for the various passbands were then aligned using stars. Some NIR frames do not contain stellar images. In those cases we used the galaxy center to align the NIR images with the I-band frame. The center shift between I and K, due to dust extinction, is very small (numbers are given in Table 5, see § 3.5.). Only for NGC 5866 (M 102) was this procedure especially difficult, due to the fact that a very strong dustlane obscures the center even in K. Given the lack of colour structures across stellar images in the colour maps, we estimate that the alignment is accurate to of order 0.2".

3.3. Bulge colours and colour gradients

Paper I describes how we determine bulge optical colours and colour gradients. We use the same approach for the determination of near-infrared colours and gradients. Briefly, we follow the following steps.

First, we determine the galaxy center as the central luminosity peak of the K-band galaxy image. With the exception of NGC 5866, whose prominent dust lane has been described in the previous section, the K-band peak always lies at the center of symmetry of the galaxy, as determined by ellipse fitting to the entire bulge region. The K-band peak is thus a suitable choice of center.

Second, we determine the galaxy's orientation on the sky by fitting ellipses to the K-band frames. For these highly inclined galaxies the disk major axis orientation is well constrained by the ellipticity profile, which becomes flat in the outer parts. The orientation of each galaxy is given in Table 1 as the position angle of the semi-minor axis which shows the least amount of dust obscuration (see below).

Once center and orientation are determined, we extract surface brightness profiles on both semi-minor axes. We use azimuthal averages on wedge-shaped apertures with full-width 22.5°. Colour profiles are determined by subtracting calibrated profiles from each other. Appendix A gives the wedge surface brightness profiles in R and the colour profiles, in tabular and graphical form, for the two semi-minor axes of each galaxy.

As a result of the high inclination of our sample, colour structures associated to reddening by dust in the disk are commonly seen on one semi-minor axis of each galaxy. On the opposite semi-minor axis the colour profiles are generally featureless and scale-free, ie. linear when plotted against $\log(r)$.

To determine bulge central colours and colour gradients we fit a linear relation to the colour profiles between an inner and an outer radius, as described in BP94. We used a minimum inner cutoff radius of 1 seeing FWHM, to avoid any effects of seeing and bad centering, but in cases where the colour gradients changed significantly inside the bulge, we moved the inner cutoff out to the radius where this change occurred. Changes like this can be caused by dust extinction in the nuclear area, or by a change in stellar populations, similar to elliptical galaxies (e.g. Surma & Bender 1995). We put the outer radius at the place where, according to a bulge-disk decomposition, 50% of the light comes from the bulge. In some galaxies with large bulges the outer radius was set at 30". The inner and outer radii are listed in Table 2, where we also present the bulge colour gradients. The optical gradients presented here are not identical as those presented in BP94, especially as a result of different centering and sometimes different inner radii, but the differences are small, and give an indication of the error in these measurements. The errors presented in Table 3 are formal errors of the fit.

To give characteristic values for the bulge and disk colours we follow the convention we use in the previous papers in this series, namely we extract the bulge colours at 0.5 $r_{\rm eff}$, or 5", if this was larger, and the disk colours at 2 major axis K-band scale lengths. Table 3 lists the characteristic colours of bulges and disks. The effective radii of the bulges in K have been determined from the two-dimensional bulge-disk decomposition of the K-band frames in APB95; they are very similar, but not identical, to those given in BP94.

3.4. Disk surface brightness, colours and scale length ratios

For the extraction of disk surface brightness distributions, we center wedge apertures slightly away (15°) from each semi-major axis, on the least dusty side; major-axis apertures often cut over strong dust lanes on the disk, which we want to avoid. The disk apertures have a full-width of 10°. Using the K-band center we average azimuthally the light in the wedge. Colour profiles are determined by subtracting calibrated profiles from each other. The profiles for the two wedges are finally averaged. The difference between the profiles for the two wedges is the main source of uncertainty on the disk surface brightness profile; the profiles do not reach the disk faint outer parts hence sky uncertainty does not contribute to surface brightness errors. We call these near-major-axis profiles the "disk profiles" although, clearly, bulge light contributes in the central parts. No geometric scaling has been applied to project the profiles to the major axis. Such scaling is applied later whenever needed, eg. for the determination of disk scale lengths. Colour profiles are derived from the ratios of surface brightness profiles. We give surface brightness and colour profiles for the disk profiles in tabular and graphical form in Appendix A.

We next measure the colour gradients in the disk by fitting linear laws to the colour profiles against linear radius. The results from the fit are given in Table 4. The gradients are presented per projected

Table 2: Bulge colour gradients

NGC	Fitting Range (arcsec)		$\nabla(B-R)$	$\pm$	$\nabla(U-R)$	$\pm$	$\nabla(R-K)$	$\pm$	$\nabla(R-I)$	$\pm$	$\nabla(J-K)$	$\pm$
(1)	(2)	(3)	(4)	(5)	(6)	(7)	(8)	(9)	(10)	(11)	(12)	(13)
5326	1.8	10.5	-0.21	0.02	-0.33	0.02	-0.34	0.04	0.00	0.02	-0.19	0.02
5362	1.6	6.0	-0.10	0.02	-0.35	0.03	-0.13	0.04	-0.14	0.02		
5389	3.0	14.0	-0.18	0.03	-0.41	0.06	-0.15	0.01	0.02	0.02	0.03	0.01
5422	2.0	14.0	-0.15	0.02	-0.31	0.01	-0.17	0.02	-0.04	0.02	-0.09	0.01
5443	5.0	10.0	-0.13	0.06	-0.38	0.07	-0.30	0.04	-0.10	0.13	0.13	0.06
5475	3.0	11.0	-0.10	0.06	-0.36	0.05	-0.38	0.08	-0.11	0.07	-0.18	0.03
5577	1.5	11.0	-0.43	0.02	-0.85	0.04	-0.44	0.05	-0.15	0.02	-0.08	0.03
5587	1.5	20.0	-0.33	0.02	-0.73	0.04	-0.15	0.06	-0.07	0.02		
5675	5.0	10.2	-0.22	0.07			-0.25	0.06	-0.02	0.04		
IC 1029	2.5	10.6	-0.45	0.03	-0.77	0.10	-0.20	0.04	-0.09	0.04		
5689	3.0	10.0	-0.08	0.01	-0.27	0.02	-0.22	0.02	-0.04	0.02	0.04	0.02
5707	1.6	7.2	-0.35	0.02	-0.62	0.02	-0.07	0.02	-0.06	0.01		
5719	1.4	12.0	-0.34	0.02	-0.61	0.04	-0.75	0.02	-0.12	0.01		
5746	2.5	21.0	-0.25	0.01	-0.50	0.02	-0.32	0.02	-0.12	0.01	-0.10	0.01
5838	3.0	20.0	-0.10	0.02	-0.28	0.02	-0.13	0.01	-0.09	0.01	-0.02	0.01
5854	1.4	9.2	0.11	0.02	-0.03	0.01	-0.12	0.01	-0.11	0.02	0.03	0.01
5866	6.0	15.0	-0.15	0.02	-0.30	0.03	-0.30	0.04	-0.10	0.02	-0.07	0.04
5879	1.6	7.0	-0.40	0.03	-1.00	0.03	-0.65	0.02	-0.24	0.01	-0.27	0.02
5908	9.0	30.0	-0.03	0.07	-0.08	0.07	0.01	0.10	-0.05	0.08		
5965	1.4	11.0	-0.17	0.02	-0.35	0.04	-0.29	0.03	-0.10	0.01	0.05	0.01
5987	1.5	13.0	0.08	0.01	-0.15	0.02	-0.35	0.02	-0.24	0.02	-0.08	0.02
6010	1.4	6.0	-0.26	0.01	-0.62	0.02	-0.30	0.03	-0.01	0.02	-0.04	0.02
6368	1.5	10.0	-0.24	0.03	-0.28	0.10	-0.20	0.01	-0.04	0.02	-0.03	0.02
6504	1.7	8.1	-0.15	0.01	-0.27	0.01	-0.01	0.02	-0.04	0.02		
6757	1.7	8.0	-0.11	0.02	0.02	0.03	-0.24	0.04	-0.25	0.02		
7311	1.6	15.0	-0.43	0.03	-1.10	0.09	-0.24	0.04	-0.22	0.03		
7332	1.5	8.2	0.10	0.03	-0.18	0.02	-0.32	0.03	-0.26	0.03	-0.04	0.01
7457	1.3	20.0	0.08	0.02	0.08	0.02	-0.25	0.01	-0.04	0.01	-0.06	0.01
7537	2.0	12.0	-0.44	0.05	-0.49	0.07	-0.43	0.06	-0.03	0.02	-0.18	0.05
7711	1.4	11.5	-0.17	0.03	-0.27	0.02	-0.26	0.02	-0.14	0.02	-0.13	0.01

Notes to table 2: Description of the columns:
Columns (2) and (3) display the radial range on the minor axis used to fit the bulge color gradients. Columns (4), (6), (8), (10) and (12) show the gradient of colour against logarithmic radius $\Delta(Colour)/\Delta(\log\ r)$. In columns (5), (7), (9), (11) and (13) the formal error of this fit is given.

Table 3: Colours of bulges and disks

Galaxy	$(B-R)_B$	$(B-R)_D$	$(U-R)_B$	$(U-R)_D$	$(R-K)_B$	$(R-K)_D$	$(J-K)_B$	$(J-K)_D$
5326	1.444	1.405	1.946	1.845	2.604	2.56	0.874	0.911
5362	1.144	0.97	1.46	1.012	2.414	2.274	–	–
5389	1.439	1.434	1.741	1.772	2.678	2.662	0.874	0.921
5422	1.462	1.376	1.901	1.804	2.704	2.709	0.867	0.913
5443	1.521	1.354	2.057	1.776	2.461	2.485	0.931	0.925
5475	1.474	1.506	1.876	1.885	2.498	2.474	0.867	0.883
5577	1.3	1.061	1.235	0.821	2.539	2.171	0.835	0.589
5587	1.471	1.423	1.914	1.777	2.564	2.602	–	–
5675	1.472	1.329	–	–	2.58	2.458	–	–
IC 1029	1.402	1.25	1.808	1.614	2.492	2.52	–	–
5689	1.437	1.482	1.861	1.896	2.705	2.638	0.902	0.918
5707	1.53	1.328	1.874	1.629	2.711	2.588	–	–
5719	1.61	1.402	2.059	1.759	2.933	2.435	–	–
5746	1.595	1.65	2.162	2.214	2.821	2.851	0.982	0.979
5838	1.488	1.435	2.039	1.871	2.725	2.679	0.866	0.838
5866	1.451	1.457	1.841	1.682	2.609	2.44	0.863	0.94
5854	1.392	1.442	1.742	1.79	2.48	2.495	0.922	0.781
5879	1.271	1.314	1.279	1.293	2.404	2.476	0.779	0.833
5908	1.441	1.547	1.765	1.908	2.595	2.984	–	–
5965	1.408	1.444	1.978	2.038	2.667	2.731	0.901	0.962
5987	1.49	1.477	1.962	1.886	2.966	2.667	1.18	1.074
6010	1.435	1.504	1.805	1.759	2.535	2.66	0.954	1.046
6368	1.723	1.607	2.031	1.91	3.121	2.976	0.896	0.929
6504	1.789	1.746	2.118	1.721	2.633	2.381	–	–
6757	1.434	1.38	1.672	1.46	2.707	2.76	–	–
7311	1.523	1.348	1.963	1.479	2.827	2.726	–	–
7332	1.353	1.413	1.802	1.753	2.393	2.165	0.829	0.658
7457	1.287	1.325	1.675	1.618	2.403	2.172	0.862	0.829
7537	1.285	1.242	1.267	1.138	2.593	2.379	0.875	0.866
7711	1.405	1.464	2.022	2.083	2.653	2.551	0.901	0.838

Notes to table 3: Bulge colours are given at 0.5 r_{eff} or at 5", whichever larger, on the minor axis. Disk colors are given at two major axis K-band scale lengths, and have been measured using the major axis 'dustfree' wedges.

K-band scale length, also given in Table 4. The radial range is chosen in such a way that we fit the exponential colour gradients outside the region of the bulge, and that a radial region is as large as possible and present in all passbands. In any case, we don't see strong variations in slope of colour as a function of radius when going from the bulge to the disk (see Appendix A and PB96a). The fitting range is the same for each passband.

3.5. Center shifts

A useful indicator for the presence of dust in inclined galaxies is the change in the position of the center as a function of wavelength. This shift occurs when a dustlane in front of the center of light obscures more light on one side of the center than on the other, causing the observed center to shift as a function of optical depth, or passband. In Table 5 we give the shift of the peak in arcsec between the K-band and the other bands. Shifts are approximately along the minor axis. Typical errors, including the uncertainty of the determination of the luminosity peaks and the errors of alignment, are 0.2–0.3 arcsec. We plot the shifts as a function of reciprocal wavelength in Fig. 1, showing that they increase with μ^{-1} in an approximately linear way.

3.6. Comparison with other authors

In BP94 we compared our optical data with various sources from the literature. Here we compare the infrared data.

3.6.1. Comparison with literature surface photometry

Since de Jong's sample is orientated towards face-on galaxies and ours towards edge-on, there is no overlap between the two samples. We have 4 galaxies in common with Terndrup *et al.* (1994). For the comparison we have determined elliptically averaged major axis profiles in the same way as was done by Terndrup *et al.* (1994) and then made the comparison (see Fig. 2), with their corrected data (see Terndrup *et al.* (1995). The differences near the center can be explained well by the fact that our seeing and sampling was better than that of Terndrup *et al.* (1994). In the outer parts of NGC 7457 the difference might be explained by sky background errors, since their field was smaller. However, there seems to be a general offset between the two datasets, of about 0.05 - 0.10 mag, in the sense that the profiles of Terndrup *et al.* are fainter. This is however not the case for NGC 7332, the best studied galaxy.

As for the colour profiles, we have 3 galaxies in common in $J-K$ and one in $R-K$, and here the agreement is better than 0.1 mag, except near the center.

3.6.2. Comparison with aperture photometry

As a check on our photometric calibration we compare our data to aperture photometry from the literature. The literature photometry is from the compilation by de Vaucouleurs & Longo (1988). We find

Table 4: Disk parameters

NGC	Fitting Range		h_K	±	$(B-R)_0$	$\frac{\Delta(B-R)}{\Delta(h_K)}$	$(U-R)_0$	$\frac{\Delta(U-R)}{\Delta(h_K)}$	$(R-K)_0$	$\frac{\Delta(R-K)}{\Delta(h_K)}$	$(R-I)_0$	$\frac{\Delta(R-I)}{\Delta(h_K)}$	$(J-K)_0$	$\frac{\Delta(J-K)}{\Delta(h_K)}$
(1)	(2)	(3)	(4)	(5)	(6)	(7)	(8) 7 (9)	(10)	(11)	(12)	(13)	(14)	(15)	
5326	15	45	9.1	0.1	1.61	-0.05	2.23	-0.12	3.28	-0.22	0.66	0.02	0.88	0.01
5362	10	40	9.2	0.1	1.24	-0.08	1.55	-0.18	2.63	-0.16	0.60	-0.05		
5389	15	40	17.9	1.9	1.79	-0.04	2.11	0.00	3.02	0.05	0.93	-0.05	1.00	-0.05
5422	10	45	10.9	0.1	1.66	-0.06	2.20	-0.08	2.71	-0.01	0.70	0.00	0.84	0.01
5443	10	45	17.6	0.3	1.55	-0.10	2.18	-0.31	2.64	-0.09	0.61	0.04	0.93	0.07
5475	10	40	9.0	0.1	1.53	-0.04	1.94	-0.03	2.50	-0.03	0.65	-0.03	0.84	-0.01
5577	10	45	20.5	0.1	1.42	-0.18	1.28	-0.14	2.80	-0.19	0.61	-0.01	1.00	-0.12
5587	15	45	8.4	0.1	1.71	-0.10	2.25	-0.20	3.02	-0.12	0.74	-0.07		
IC 1029	10	35	9.6	0.1	1.98	-0.31	2.48	-0.38	3.45	-0.23	0.84	-0.07		
5675	10	45	11.3	0.4	1.75	-0.17			2.92	-0.22	1.00	-0.18	2.64	-0.30
5689	15	45	11.4	0.3	1.85	-0.12	2.45	-0.28	3.16	-0.29	0.79	-0.06	1.04	-0.06
5707	10	45	12.6	0.1	1.67	-0.15	2.10	-0.17	2.74	0.01	0.75	-0.05		
5719	15	45	10.7	0.4	2.29	-0.21	2.95	-0.28	3.57	-0.20	0.85	-0.07		
5746	10	35	16.4	0.8	2.29	-0.24	3.14	-0.57	3.01	0.71	0.78	0.11	0.83	0.31
5838	15	45	17.9	0.2	1.50	-0.01	2.22	-0.11	2.83	-0.09	0.66	-0.01	0.88	0.01
5854	10	45	10.5	0.1	1.48	0.01	1.49	0.14	2.45	0.00	0.60	-0.01	0.92	0.01
5866	15	45	12.2	0.5	1.62	-0.08	1.96	-0.09	2.88	-0.14	0.65	-0.01	0.94	-0.08
5879	10	30	8.4	0.1	1.59	-0.13	1.45	-0.13	3.26	-0.31	0.65	-0.04	1.12	-0.13
5908	10	45	10.2	0.1	1.89	-0.13	1.64	-0.06	4.94	-0.53	1.19	-0.12		
5965	10	45	12.2	0.4	1.98	-0.23	3.14	-0.58	3.49	-0.17	0.92	-0.10	0.95	0.13
5987	10	45	12.6	0.3	1.95	-0.04	2.79	-0.15	3.95	-0.29	0.89	-0.05	1.30	0.01
6010	10	45	11.5	0.2	1.55	0.00	2.21	-0.18	2.56	0.04	0.66	-0.03	0.80	0.15
6368	10	40	13.2	0.3	1.93	-0.20	2.48	-0.38	3.34	-0.16	0.87	-0.09	0.86	0.08
6504	15	45	14.4	0.2	1.92	-0.11	2.51	-0.24	2.87	-0.09	0.77	-0.08		
6757	10	45	9.9	0.1	1.57	-0.06	1.92	-0.04	2.73	0.01	0.57	0.00		
7311	10	40	9.0	0.1	1.73	-0.08	2.47	-0.25	3.12	-0.14	0.81	-0.05		
7332	10	35	11.4	0.3	1.46	-0.06	1.96	-0.08	2.46	-0.04	0.52	-0.01	0.95	-0.12
7457	10	45	16.0	0.1	1.36	-0.04	1.79	-0.06	2.47	-0.11	0.57	-0.01	0.89	-0.06
7537	15	30	8.8	0.6	1.43	-0.11	1.60	-0.25	2.97	-0.25	0.85	-0.17	1.27	-0.11
7711	10	40	10.1	0.1	1.54	-0.05	2.12	-0.08	2.67	0.00	0.58	0.02	0.91	0.02

Notes to table 4: In columns (2) and (3) the fitting range along the wedge is given in arcsec. Columns (4) and (5) give the K-band scale length in arcsec, calculated using the average of the 2 wedges at 15° from the major axis on the 'dustfree' side, and its formal fit error. To obtain the major axis scale length, multiply this number by 1.03. In columns (6), (8), (10), (12) and (14) are given the extrapolated central colors of the disk, as fitted. Columns (7), (9), (11), (13) and (15) contain the color gradients, along a wedge aperture at 15° from the major axis, per K-band scale length.

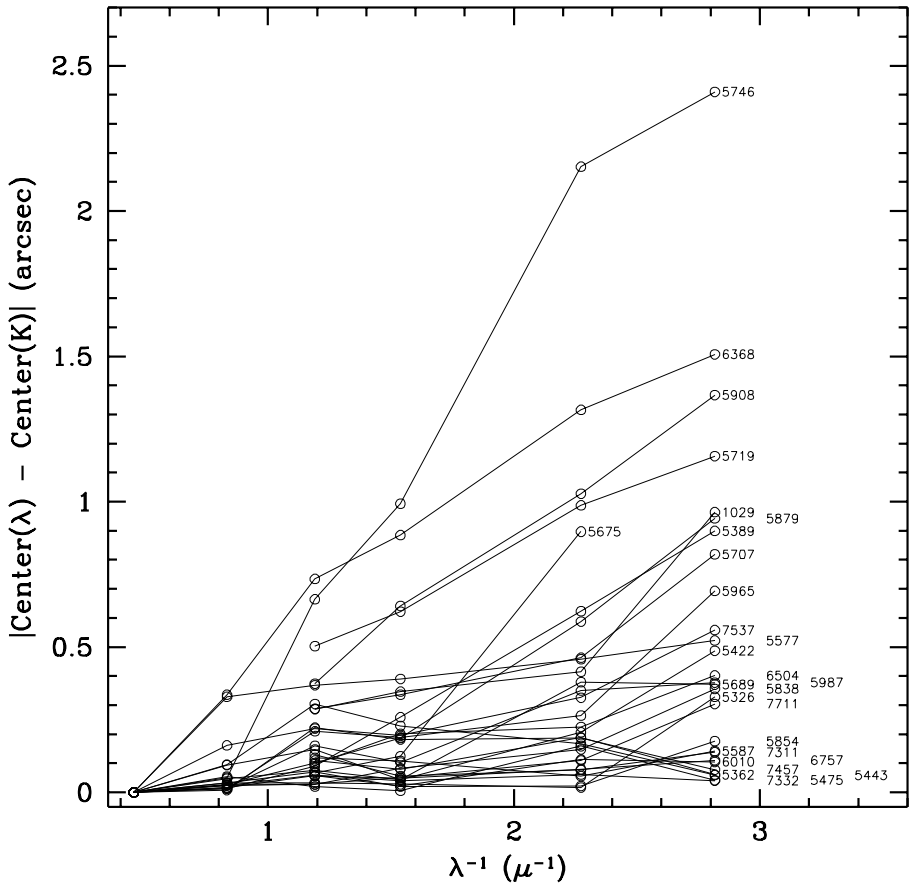

Fig. 1.— Shift of the position of the galaxy center as compared to the K-band, plotted against reciprocal wavelength.

Table 5: Shifts of the galaxy luminosity peaks with respect to the K-band position

NGC	Δ(JK) (arcsec)	Δ(IK) (arcsec)	Δ(RK) (arcsec)	Δ(BK) (arcsec)	Δ(UK) (arcsec)
5326	0.032	0.033	0.028	0.017	0.328
5362	–	0.109	0.080	0.188	0.061
5389	0.012	0.090	0.258	0.623	0.899
5422	0.047	0.075	0.043	0.206	0.487
5443	0.095	0.304	0.229	0.167	0.059
5475	0.054	0.020	0.005	0.159	0.042
5577	0.328	0.369	0.390	0.458	0.522
5587	–	0.118	0.108	0.055	0.142
5675	–	0.066	0.124	0.897	–
IC 1029	–	0.286	0.346	0.415	0.964
5689	0.094	0.148	0.044	0.379	0.371
5707	–	0.288	0.336	0.463	0.819
5719	–	0.503	0.622	0.987	1.157
5746	0.050	0.664	0.993	2.152	2.410
5838	0.025	0.027	0.082	0.148	0.356
5866	–	–	–	–	–
5854	0.032	0.070	0.020	0.022	0.176
5879	0.027	0.101	0.187	0.588	0.942
5908	–	0.374	0.641	1.028	1.367
5965	0.012	0.210	0.188	0.264	0.693
5987	0.016	0.160	0.103	0.350	0.378
6010	0.017	0.057	0.022	0.113	0.105
6368	0.335	0.734	0.885	1.316	1.507
6504	–	0.097	0.201	0.225	0.402
6757	–	0.056	0.049	0.079	0.110
7311	–	0.130	0.056	0.077	0.138
7332	0.023	0.059	0.040	0.061	0.040
7457	0.008	0.222	0.182	0.187	0.078
7537	0.161	0.220	0.195	0.326	0.558
7711	0.023	0.028	0.050	0.109	0.304

aperture data for 5 of our galaxies. On the average, our magnitudes are 0.145 mag brighter in J and 0.061 in K. Table 6 gives the differences (literature magnitudes minus ours) for the 5 galaxies.

The differences are larger than expected from the scatter in the standard stars, and consistent with the surface brightness comparisons. They are, certainly in K, small enough that they don't affect the final interpretation of the colours. The source of the discrepancies is unclear. We have rerun the entire reduction process as a check, without applying a linearity correction to the data, and obtained the same results. It should be noted that the effects of seeing on surface brightness profiles of highly-inclined galaxies are stronger than on round galaxies. Also, the total number of aperture measurements is only 13 in each band. Both arguments together show that the discrepancy is minor, especially if the errors in the literature surface photometry are underestimated.

4. Discussion & Conclusions

In this data paper we present high-quality surface photometry for a sample of early-type spiral galaxies in 6 bands, ranging from U (3700 Å) to K (2.2 μm). The galaxies comprise a complete optically selected sample of inclined spirals of type S0 – Sbc. It is ideal to study the stellar populations of bulges, since the bulges of early-type spirals are large, and in general only one side of the bulges is obscured by the disk, so that the other is relatively free of extinction by dust and of contamination by the disk. The infrared data have been obtained with a 256 $\times$ 256 InSb array with a field of $\sim$ 80 $\times$ 80 arcsec, more than enough to contain the whole bulge, and the inner galaxy disk. The effective seeing is approximately 1″ in the infrared and 1.5 ″ in the optical. Our photometry has been extensively compared with the literature in BP94 (for the optical) and in this paper (for the infrared). For the surface brightness profiles the agreement is good. The absolute calibration is accurate to 0.10 mag in U and B, 0.05 in R and I, and 0.10 mag in J and K. We provide surface brightness and colour profiles for the individual galaxies, as well as measurements of absolute magnitudes, bulge-to-disk ratios, bulge effective radii, disk scale-lengths, mean colours of bulges and disks, colour gradients of bulges and disks, and center shifts in each passbands.

The sample may serve as a standard sample for the colours of galactic bulges, replacing the work of Persson *et al.* (1979) and Frogel *et al.* (1978). It is complementary to the sample of de Jong & van der Kruit (1994) in inclination, and to the sample of Peletier *et al.* (1994) in galaxy types. It has similar selection criteria as the sample of Terndrup *et al.* (1994).

Table 6: Comparison with aperture photometry

Galaxy	Nr. of measurements	Δ J	Δ K
(1)	(2)	(3)	(4)
NGC 5746	6	0.166	0.106
NGC 5879	1	0.189	0.074
NGC 5987	3	0.119	-0.031
NGC 7332	2	0.064	0.053
NGC 7537	1	0.189	0.101

Note: Δ=literature mean minus this paper.

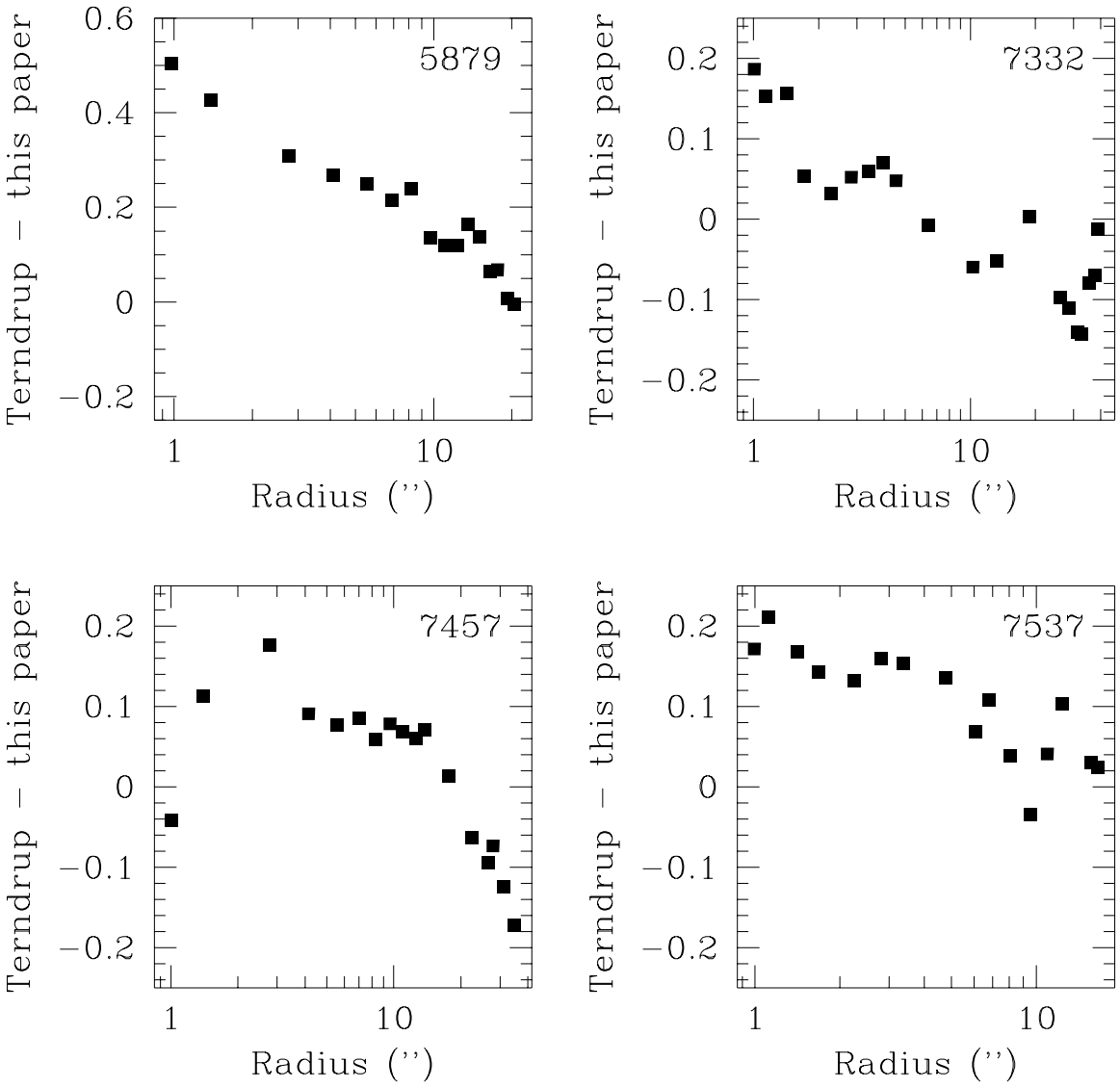

Fig. 2.— Comparison with the K-band major axis profiles of Terndup *et al.* (1994).

This is the first study of a moderately large number of galactic bulges based on NIR data using 256 × 256 arrays. Compared to the recent study of Terndrup *et al.* (1994), based on 58 × 62 InSb array data, our spatial sampling in the center is higher, the photometry goes out further, and we cover more passbands (we also give U, B and I). Colours are treated in more detail in our paper. In particular, we present minor axis colour profiles, which allow for the study of bulge colours unaffected by extinction.

We wish to use the electronic format of *New Astronomy* to present all the calibrated images and colour maps electronically for easy access and further processing by the community. We are confident that this will contribute to the furthering of our understanding of the structure and formation history of galaxy bulges.

Acknowledgements

This article is based on observations taken at the United Kingdom Infrared Telescope in Hawaii, operated by the Royal Observatory Edinburgh on behalf of PPARC, and from the Isaac Newton Telescope, operated by the RGO, on behalf of PPARC, at the Observatorio del Roque de los Muchachos of the Instituto de Astrofísica de Canarias. This research has made use of the NASA/IPAC Extragalactic Database (NED) which is operated by the Jet Propulsion Laboratory, California Institute of Technology, under contract with the National Aeronautics and Space Administration. The authors thank A. Vazdekis and M. Stiavelli for help with the observations and A. Akalin for help with preparing the electronic manuscript.

Appendix A

In this appendix we present three sets of figures, and four sets of tables, which together form the whole available database on the surface photometry of the inner parts of these galaxies.

Fig. 3.— Broad-band images of all the galaxies, in U, B, R, I, J and K, in GIF or FITS format. Images are flatfielded, calibrated, scaled and registered. To download, click on the word 'FITS' and save to a local file.

Fig. 4.— $U - R$ and $R - K$ colour index maps for all the galaxies, in GIF format. True-colour URK composite images. See text.

Fig. 5.— Colour index profiles for each galaxy, along the two semi-minor axes and along two axes 15^{o} away from the major axis on the less-dusty side of each galaxy. The vertical dotted line is placed at 1 seeing FWHM. The two vertical solid lines indicate the limits of the range used for the measurement of the colour gradients.

Figure 3 contains FITS-format copies of the flatfielded, calibrated, scaled and registered broad-band images of the galaxies in U, B, R, I, J and K. Magnitudes corresponding to 1 ADU in each passband are given in the FITS header keyword PHOTCON. Pixel scale is 0.549 arcsec/pixel.

Figure 4 contains GIF format copies of the $U-R$ and $R-K$ colour index maps, and a GIF format "true-colour" URK composite. In the colour index images, blue-red-yellow correspond to increasingly higher values of the colour index. The colour scale has been independently adjusted in each image to highlight the morphological components in the colour index maps. The true colour URK images are built using photometrically-calibrated K, R, and U frames as RGB colours. The colour scheme is the same for all the galaxies, ie. colour index comparisons among galaxies can be performed directly from the colours seen in these images. We have published a composite of the true-colour images of the entire sample in PB96a.

Colour profiles along the minor and (near)-major axes are plotted in Figure 5. The derivation of the profiles is described in § 3.3. for the bulges and § 3.4. for the disks. In each panel, each set of symbols corresponds to a different wedge aperture. The vertical dotted line is drawn at 1 seeing FWHM. The two vertical solid lines indicate the inner and outer limits of the range used for measuring colour gradients.

Table 7 gives the R-band surface brightness and the colour profiles for all the galaxies in the sample, along the semi-minor axis where the dust effects are less pronouced ('dustfree' side). The first column gives the radius in arcsec. Subsequent columns are in magnitudes per square arcsec. Errors, given in the $\pm$ columns, are in the same units. The header of each table gives the NGC number of the galaxy and the position angle of the semi-minor axis.

Surface brightness and colour profiles along the other, more dusty semi-minor axis of each galaxy are given in Table 8. The headers of these tables give the position angle, and a "D" denoting 'dusty side'.

Table 9 gives the R-band near-major-axis surface brightness and colour profiles for all the galaxies. The first column gives the radius in arcsec along an axis 15$^{\rm o}$ away from the disk major axis. Subsequent columns are in magnitudes per square arcsec and represent the surface brightness azimuthally averaged in the two wedges on the 'dustfree' side. The error in the next column is half the difference between the two wedges.

Table 10 gives the elliptically-averaged surface brightness in K as a function of major axis radius, together with the ellipticity (1-b/a), the position axis of the major axis, and the 4th order Fourier terms s4 and c4 (Carter 1980). In the outer parts the ellipse shape has been kept constant, so that the surface brightness is less affected by errors in those parameters. These parameters have been fitted on the original K-band images, with a pixelsize of 0.291", contrary to tables 7, 8 and 9, which derive from NIR data rebinned to the larger, 0.549" pixel size of the optical data.

REFERENCES

Andredakis, Y.C., Peletier, R.F. & Balcells, M., 1995, MNRAS, 275, 874 (APB95)

Balcells, M., Peletier, R. F. 1994, AJ, 107, 135 (BP94)

de Vaucouleurs, G., de Vaucouleurs, A., Corwin, H. G., Buta, R. J., Paturel, G. & Fougué, P., 1991, *Third Reference Catalogue of Bright Galaxies*, New York, Springer. (RC3)

de Vaucouleurs, A. & Longo, G. 1988, *The Catalogue of Visual and Infrared Photometry of Galaxies from 0.5 μm to 10 μm*, Austin, Univ. of Texas Press.

de Jong, R., S., van der Kruit, P. C. 1994, A&AS, 106, 451

de Jong, R., 1996, A&AS, in press

Kent, S. 1984, ApJS, 56, 105

Kent, S. 1986, AJ, 91, 1301

Kent, S. 1987, AJ, 93, 816

Lauberts, A. & Valentijn, E.A., 1989, *The Surface Photometry Catalogue of the ESO Sky Survey*, ESO, Garching

Peletier, R.F., 1993, A&A, 271, 51

Peletier, R. F., Valentijn, E.A., Moorwood, A.F.M. & Freudling, W., 1994, A&AS, 108, 621

Peletier, R. F., Balcells, M. 1996, AJ, 111, 2238 (PB96a)

Peletier, R. F., Balcells, M. 1996, in *Spiral Galaxies in the near-IR*, eds. D. Minnitti, H.-W. Rix, Springer-Verlag, p. 48 (PB96b)

Puxley, P. & Aspin, C., 1994, Spectrum, 2, 4

Surma, P. & Bender, R., 1995, A&A, 298, 405

Terndrup, D. M., Davies, R. L., Frogel, J. A., DePoy, D. L., Wells, L. A. 1994, ApJ, 432, 518

Terndrup, D. M., Davies, R. L., Frogel, J. A., DePoy, D. L., Wells, L. A. 1995, ApJ, 454, 945